



Cite this: DOI: 10.1039/c8gc02221f

Sustainable visible light assisted *in situ* hydrogenation *via* a magnesium–water system catalyzed by a Pd-g-C₃N₄ photocatalyst†

Priti Sharma * and Yoel Sasson

A non-hazardous and relatively mild protocol was formulated for an effectual hydrogen generation process *via* a “magnesium-activated water” system with a Pd-g-C₃N₄ photocatalyst under visible light at room temperature. Water functions photochemically as a hydrogen donor without any external source with the Pd-g-C₃N₄ photocatalyst. The synthesized Pd-g-C₃N₄ photocatalyst is highly efficient under visible light for the selective reduction of a wide range of unsaturated derivatives and nitro compounds to afford excellent yields (>99%). The photocatalyst Pd-g-C₃N₄ could be easily recovered and reused for several runs without any deactivation during the photochemical hydrogen transfer reaction process.

Received 17th July 2018,
Accepted 24th October 2018

DOI: 10.1039/c8gc02221f

rsc.li/greenchem

Introduction

The hydrogenations of unsaturated hydrocarbons and nitro groups are vital reactions in organic synthesis; both processes are extensively used in the production of fine chemicals, fragrances, pharmaceuticals and agrochemicals.¹ Over the past few decades, a considerable amount of effort has been devoted to the area of catalytic hydrogenation using hydrogen (H₂) gas.² However, hydrogen generation, storage, and transportation are highly hazardous and costly, and require special facilities.³ An efficient utilization of solar energy could mitigate many energy and environmental issues *via* direct conversion of light energy into chemical energy.⁴ In the same context, photocatalytic hydrogen generation from water splitting using semiconductors has attracted worldwide attention for promising green production of hydrogen gas.⁵ In a notable work, J. Song and B. Han stated that nitrobenzenes could be reduced to the corresponding anilines with high selectivity by the H₂ from water splitting and glucose reforming *via* Pd/TiO₂ under UV irradiation (350 nm).⁶ Recently, in another notable work, B. Török *et al.* reported chemoselective reduction of a broad variety of functional groups by a Pd/C–Al–H₂O system successfully (24 h, high T).⁷ In a different approach, reagents (MgH₂, MgLiBH₄, CH₃OH, diborane)⁸ were also reported for H₂ generation; but typically under harsh reaction conditions.

Nevertheless these reported processes call for laborious synthesis procedures with the use of costly ligands and noble metals.⁹ Recently, a g-C₃N₄ semiconductor exhibited interesting physicochemical attributes namely visible light activity, high stability, nontoxicity, metal free organocatalysis, simple fabrication and material inertness¹⁰ which make it the best fit for unique photocatalytic activity from the environmental and economic perspectives.¹¹ In the last few years, our research group demonstrated water activation through reducing metals (Zn, Mg and Fe) provides a “green” source of H₂ for hydrogen transfer reactions, however the drawback of the reaction is the use of a high temperature and time-consuming protocol.¹² Out of the above list, Mg–H₂O is the preferred reagent due to its safety, versatility, environmental benignancy and ease of handling.

Herein, we describe for the first time a pressure free, mild photochemical protocol for selective reduction of olefin and nitro compounds using a non-hazardous, abundant, and eco-friendly “H₂O–Mg” pair as a H₂ donor in the presence of a Pd-g-C₃N₄ photocatalyst at room temperature (Scheme 1). The new reaction system is a more expedient and greener protocol compared to earlier studies.^{12c,13}

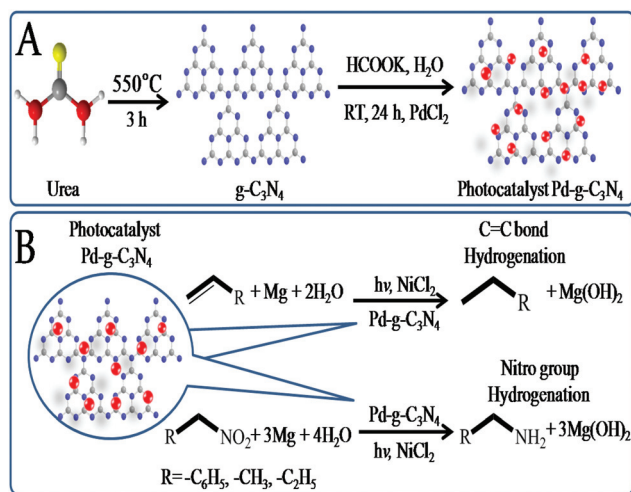
Results and discussion

g-C₃N₄ was fabricated *via* the known procedure of Wei Chen.^{10a,14} The photocatalyst Pd-g-C₃N₄ was prepared by stirring PdCl₂ with g-C₃N₄ in water in an open round bottom flask until dry for 24 h (ESI 1a and b) (Fig. S1†) (Scheme 1A).

The typical X-ray diffraction (XRD) patterns of (a) g-C₃N₄ and (b) Pd-g-C₃N₄ materials are shown in Fig. 1. For the pure

Casali Center of Applied Chemistry, Institute of Chemistry, The Hebrew University of Jerusalem, Jerusalem 91904, Israel. E-mail: priti.sharma@mail.huji.ac.il

† Electronic supplementary information (ESI) available: Physical appearance, reaction setup, FT-IR spectra, nitrogen adsorption–desorption isotherm, XPS spectra, TEM images, TEM-EDAX pattern analysis, deuterated GC-MS chart, and water contact angle. See DOI: 10.1039/c8gc02221f



Scheme 1 (A) $g\text{-C}_3\text{N}_4$ and $\text{Pd-}g\text{-C}_3\text{N}_4$ fabrication and (B) $\text{Pd-}g\text{-C}_3\text{N}_4$ photocatalyzed hydrogenation.

$g\text{-C}_3\text{N}_4$, the two distinct diffraction peaks indexed at 13.4° and 27.2° , which are in good agreement with the reported¹⁵ values that correspond to the (100) and (002) diffraction planes of the graphitic $g\text{-C}_3\text{N}_4$ materials, respectively, as per JCPDS 87-1526 (Fig. 1A).¹⁶

The (100) plane diffraction peak at 13.4° corresponds to the interplanar structural packing (hole-to-hole nitride pores) in $g\text{-C}_3\text{N}_4$.^{10a,16} The intense XRD peak at 27.2° corresponds to the (002) plane and is attributed to the stacking of the conjugated aromatic system. The $\text{Pd-}g\text{-C}_3\text{N}_4$ material diffraction pattern (002) plane shows a low intensity compared to the $g\text{-C}_3\text{N}_4$ material, probably due to partial loading of Pd over the conjugated aromatic system unit of the $g\text{-C}_3\text{N}_4$ photoactive material (Fig. 1A).^{10a}

Fabrication of $g\text{-C}_3\text{N}_4$ and $\text{Pd-}g\text{-C}_3\text{N}_4$ was well characterized using FT-IR spectroscopy. The results are shown in Fig. S3† (a) $g\text{-C}_3\text{N}_4$ and (b) $\text{Pd-}g\text{-C}_3\text{N}_4$. In the FT-IR spectrum of $g\text{-C}_3\text{N}_4$, a broad band at nearly $3020\text{--}3500\text{ cm}^{-1}$ corresponds to the N–H

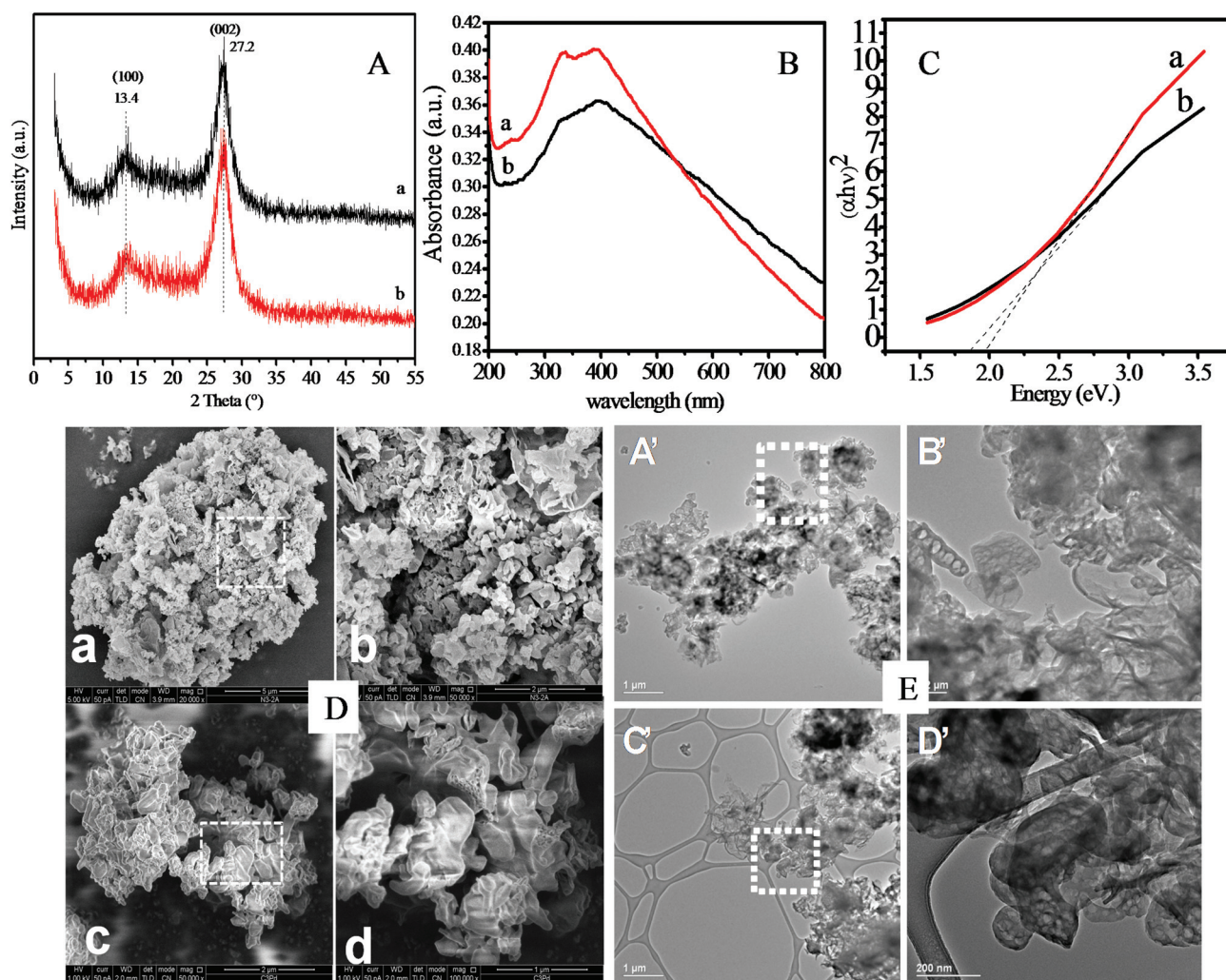


Fig. 1 (A) XRD pattern: (a) $g\text{-C}_3\text{N}_4$ and (b) $\text{Pd-}g\text{-C}_3\text{N}_4$; (B) UV-Vis spectra; (C) UV-Tauc plots, (a) $g\text{-C}_3\text{N}_4$ and (b) $\text{Pd-}g\text{-C}_3\text{N}_4$; (D) SEM images: $g\text{-C}_3\text{N}_4$ ((a) at $5\ \mu\text{m}$ and (b) at $2\ \mu\text{m}$) and $\text{Pd-}g\text{-C}_3\text{N}_4$ ((c) $2\ \mu\text{m}$ and (d) at $1\ \mu\text{m}$); and (E) TEM images: $g\text{-C}_3\text{N}_4$ at ((A') $1\ \mu\text{m}$ and (B') at $0.2\ \mu\text{m}$) and $\text{Pd-}g\text{-C}_3\text{N}_4$ ((C') at $1\ \mu\text{m}$ and (D') at $200\ \text{nm}$).

stretching vibrations of the incomplete condensed amine groups of C_3N_4 and the peaks at 1250 cm^{-1} and 1625 cm^{-1} belong to the aromatic C–N stretching vibration modes and the C–N heterocyclic stretching vibration modes, respectively (Fig. S3†).¹⁷ Additionally, the characteristic breathing mode of the triazine repeating units at 810 cm^{-1} , related to the s-triazine ring absorption band vibrations, is well observed in the fabricated $g\text{-}C_3N_4$ pale yellow material and Pd- $g\text{-}C_3N_4$.^{17c} The strong intense bands at 1625, 1550, 1410 and 1250 cm^{-1} were in good agreement with the reported literature^{10a} values of the typical stretching vibration modes of triazine derived repeating units (partial & fully condensed). After systematic loading with Pd as per the referred programme, the arrangement of all $g\text{-}C_3N_4$ molecular structures remains the same (Fig. S3†).^{17a}

The BET surface area (BET), total pore volume (V_p) and mean pore size (radius) $Dv(r)$ of $g\text{-}C_3N_4$ are found to be $15.203\text{ m}^2\text{ g}^{-1}$, 0.013 cc g^{-1} , and 15.366 \AA , respectively, however for the Pd- $g\text{-}C_3N_4$ catalyst these values are found to be $23.22\text{ m}^2\text{ g}^{-1}$, 0.018 cc g^{-1} and 17.356 \AA , respectively. The increase in the surface area (14.16%), V_p (38.46%), and $Dv(r)$ (12.95%) in Pd- $g\text{-}C_3N_4$ might be due to the transformation into monolithic sheets from bulk $g\text{-}C_3N_4$ (Fig. S5†).^{10a}

In the SEM analysis of $g\text{-}C_3N_4$, the semiconductor seems to be aggregated, whereas Pd- $g\text{-}C_3N_4$ shows a smaller unit of agglomeration with a denser morphology (Fig. 1D). The Pd- $g\text{-}C_3N_4$ TEM-EDX images refer to Pd loading over $g\text{-}C_3N_4$ (Fig. 1E and S6, S7†).

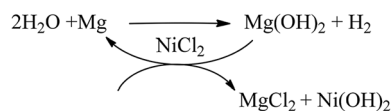
The UV-vis diffuse reflectance spectra of the prepared $g\text{-}C_3N_4$ and Pd- $g\text{-}C_3N_4$ materials were recorded and are shown in Fig. 1B and C. The $g\text{-}C_3N_4$ material spectrum indicates that the visible light absorption is ascribed to the band gap transition, corresponding to 2.0 eV for pure $g\text{-}C_3N_4$. The Pd- $g\text{-}C_3N_4$ photocatalyst shows a similar absorption pattern and shape with an observed band gap of 1.8 eV and is expected to show an increased photocatalytic performance (Fig. 1B and C).¹⁸

In the detailed XPS study, the displayed C 1s XPS spectrum shows two distinct peaks corresponding to the (–C–N–) and (–N=C–) at 284.9 and 288.3 eV, respectively, for the fabricated polymeric $g\text{-}C_3N_4$ material (Fig. S4C†).¹⁹ The N 1s spectrum of $g\text{-}C_3N_4$ clearly fitted into three separate intense peaks at 398.9, 400.1 and 401.46 eV, respectively (Fig. S4B†). The peak at 398.9 eV is assigned to the presence of pyridine-N species [sp^2 -hybridized nitrogen (C=N–C)].²⁰ The peak at 400.1 eV corresponds to nitrogen atoms trigonally bonded with the carbon (sp^2 or sp^3) atoms of amino functional groups (C–N–H). Whereas, the peak at 401.46 eV describes the terminal amino groups (–NH₂) and also attributed to charging effects or positive charge localization in heterocyclic molecules (Fig. S4D†). The catalyst shows Pd chemical states, Pd $3d_{5/2}$ at 335.16 and Pd $3d_{3/2}$ at 340.42 corresponding to Pd(0). Interestingly, the peak at 335.16 eV refers to Pd(0) of Pd- $g\text{-}C_3N_4$ and is more negative than that of normal metallic palladium from the literature, which was probably due to the electron transfer from the nitrogen atoms of $g\text{-}C_3N_4$ to Pd (Fig. S4E†).^{19a} These results suggested that Pd and the nature of the interaction between Pd and N species in the $g\text{-}C_3N_4$ might play a synergistic

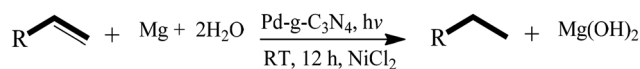
role in enhancing the performance of the catalyst for hydrogenation.²¹

Currently, an efficient photocatalytic generation of hydrogen from water under ambient conditions is one of the most challenging transformations in synthetic chemistry.^{8c} In the past few years, our research group has demonstrated that water can be activated by reducing metals (Zn, Mg, Fe) and can act as a cheap, green, abundant and universal source of hydrogen.^{12c} (Schemes 2–4). We exhibited here a pressure free, photochemical protocol for the reduction of alkenes and nitro groups using a “water/Mg” pair as a H₂ donor in the presence of the Pd- $g\text{-}C_3N_4$ photocatalyst. In a typical example, styrene (10 mmol, 1.04 g), Mg powder (15 mmol, 0.364 g), NiCl₂ (1 mmol, 0.129 g) Pd- $g\text{-}C_3N_4$ (30 mg, 0.0012 mmol 0.4% loading) and H₂O (10 mL) under visible light (15 W LED lamp, 12 cm height) were stirred in a closed glass tube and degassed under N₂ gas for 10 minutes (Schemes 2–4) for 12 h (Fig. S2†). The final reaction mixture was found to contain 99% conversion of styrene to ethyl benzene (based on the GC analysis).

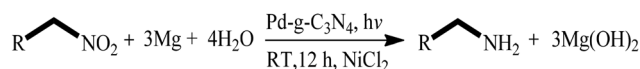
Several studies have reported^{8a,b} the addition of a trace amount of metal salts for the enhancement of H₂ generation during the Mg–H₂O reaction.^{8a,b,13} Taub *et al.* reported a crucial step to add a trace amount of metal for the enhancement of hydrogen generation during the magnesium water reaction.¹³ However, the phenomenological rate of dihydrogen formation is directly proportional to the total availability of magnesium sites, which will generally increase with higher surface area. On addition of a catalytic amount of NiCl₂, the Mg(OH)₂ oxide/hydroxide passive layer is rapidly removed from Mg metal, and the Mg surface is readily available for further reaction.^{12c,22,23} M. Chidambaram *et al.* used various metals (Mg, Fe, Ni, Zn) in terms of the amount and particle size.^{12c} It was concluded that NiCl₂ is not responsible for the chemical nature of the intermediates, but alters the physical nature (microenvironment) of the Mg layer, to facilitate the approach of the organic substrate. With the extensive established role of NiCl₂ in dihydrogen generation using the Mg/H₂O system, we



Scheme 2 Water activation via Mg metal.



Scheme 3 Olefin hydrogenation via the Pd- $g\text{-}C_3N_4$ photocatalyst.



Scheme 4 Nitro group hydrogenation via the Pd- $g\text{-}C_3N_4$ photocatalyst.

proceed with the optimized NiCl₂ usage as a physical co-catalyst (Scheme 2).

Herein, we performed a photochemical hydrogen generation reaction under visible light (15 W table LED lamp) at room temperature with 12 cm height distance from the visible light source LED lamp to the reaction mixture in a pressure glass tube to nullify the heating impact (Fig. SI-1b, S2†). The variation of different reaction parameters (dark, light, heat) demonstrated a considerable effect on the reaction over *in situ* hydrogenation of styrene, and is summarized in Table 1.

For validation of the photocatalyst Pd-g-C₃N₄, a control reaction was carried out by using only g-C₃N₄ (Table 1, entry 1), resulting in no product formation (24 h). Interestingly under visible light, the heterogeneous photocatalyst Pd-g-C₃N₄ delivered excellent reactivity to deliver the corresponding product under the optimized reaction conditions (using substrate styrene) at room temperature. The reagent Mg and cocatalyst NiCl₂ were separately used, but only 5% and 1% conversion were obtained, respectively (without PdCl₂) (Table 1, entries 3 and 4). A control reaction under dark conditions resulted in <17% of the product in 24 h (Table 1 entry 9). This experiment supports the fact that the reagent and co-catalyst alone are not sufficient for the reaction progress. These observations clearly indicate that a combination of the photocatalyst, reagent and cocatalyst (Pd-g-C₃N₄ + Mg/H₂O + NiCl₂) and visible light is critical for hydrogenation using H₂O as the H₂ source (Table 1, entries 1–13). For the further evaluation of the photocatalysis reaction, we screened the optimized reaction (using substrate styrene) under a hydrogen atmosphere under dark conditions; we observed that the reaction proceeds slowly with 41% (12 h) styrene conversion into ethylbenzene at RT (Table 1, entry 14).

Table 1 Photochemical hydrogenation reaction optimization under various parameters

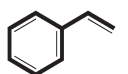
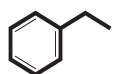
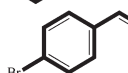
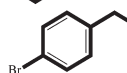
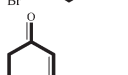
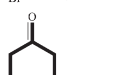
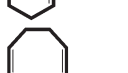
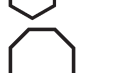
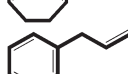
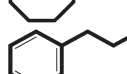
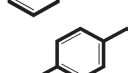
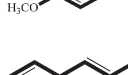
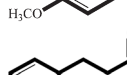
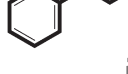
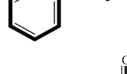
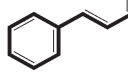
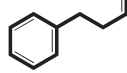
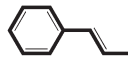
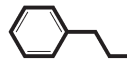
Entry	Catalyst optimization	Yield (%)	Time (h)
1	g-C ₃ N ₄	00	24
2	Pd	<2	24
3	Mg	<5	24
4	NiCl ₂	<1	24
5	Pd-g-C ₃ N ₄	<5	24
6	Mg + NiCl ₂	<2	24
7	Pd-g-C ₃ N ₄ + Mg	<15	12
8	Pd-g-C ₃ N ₄ + NiCl ₂	<3	12
9	Pd-g-C ₃ N ₄ + Mg + NiCl ₂ (in the dark)	<17	24
10	Pd-g-C ₃ N ₄ + Mg + NiCl ₂ (under visible light)	>99	12
11	Pd-g-C ₃ N ₄ + Mg + NiCl ₂ (heating at 80 °C)	>99	8
12	Pd/C (4 wt%) + Mg + NiCl ₂ (under visible light)	<8	12
13	Pd/C (4 wt%) + Mg + NiCl ₂ (heating at 80 °C)	>92	8
14	Pd-g-C ₃ N ₄ + Mg + NiCl ₂ (under dark conditions) in a hydrogen atmosphere	41	12
15	Pd-g-C ₃ N ₄ + Mg + NiCl ₂ (under visible light) in a hydrogen atmosphere	>99	8
16	Pd-g-C ₃ N ₄ + MgO + NiCl ₂ (under visible light)	>15	24

Reaction conditions: Styrene (10 mmol), Mg powder (15 mmol, 0.364 g), NiCl₂ (0.1 mmol, 0.129 g), under visible light (15 W LED lamp, 12 cm height), water (10 mL), and photocatalyst Pd-g-C₃N₄ 30 mg (0.8 wt% Pd, 0.0022 mmol).

Whereas in the presence of a light source, we found faster styrene conversion (99% in 8 h) (Table 1, entry 15). In another controlled reaction, we screened the reaction using MgO instead of Mg (under the optimized reaction conditions). The observed result with only 15% styrene conversion clearly suggests that MgO does not function well in photochemical hydrogenation (Table 1, entry 16), which might be due to NiCl₂ usage for Mg regeneration from MgO (Scheme 2).

For further evaluation of the Pd-g-C₃N₄ photocatalytic activity, various substrates were screened (Table 2). Styrene and 4-bromostyrene were successfully hydrogenated with 95% and 98% yield, respectively (Table 2, entries 1 and 2). All the screened substrates (olefin and nitro groups) have shown an appreciable yield (>99%) without any ring hydrogenation. Furthermore, non-aromatic cyclohexanone and cyclooctadiene were converted to the hydrogenated product easily with 100% and 80% yield (Table 2, entries 3 and 4). Furthermore, the reaction of monosubstituted allyl benzene and

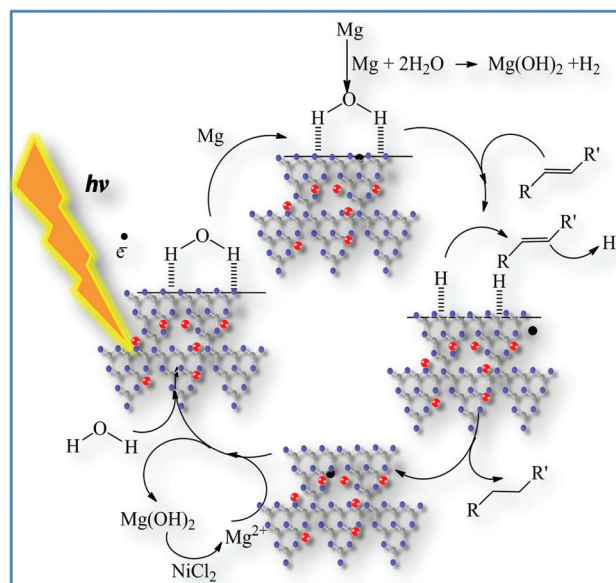
Table 2 Olefin reduction via the Pd-g-C₃N₄ photocatalyst

Entry	Substrate	Product	Yield (%)
$\text{R}-\text{CH}=\text{CH}_2 + \text{Mg} + 2\text{H}_2\text{O} \xrightarrow[\text{RT, 12 h, NiCl}_2]{\text{Pd-g-C}_3\text{N}_4, \text{h}\nu} \text{R}-\text{CH}_2-\text{CH}_2 + \text{Mg}(\text{OH})_2$			
1			95
2			98
3			100
4			80
5			92
6			90
7			90
8			90
9			85
10			99

Reaction conditions: Substrate (10 mmol), Mg powder (15 mmol, 0.364 g), NiCl₂ (0.1 mmol, 0.129 g), Pd-g-C₃N₄, 30 mg (0.8 wt% Pd, 0.0022 mmol), and water (10 mL) solvent under visible light (15 W LED lamp, 12 cm height).

disubstituted 4-allyl anisole proceeds smoothly under visible light with 92% and 90% yield without the ring hydrogenation (Table 2, entries 5 and 6). After exploring olefin hydrogenation, we proceed with the hydrogenation of the nitro group to the corresponding amines. 4-Nitrotoluene and 4-nitro benzoic acid were converted into amine substituted groups with 95% and 90% conversion, respectively (Table 3, entries 1 and 2). Furthermore, the aryl halide substituted aromatic nitro group *via* 4-iodo nitrobenzene, 4-bromo nitro benzene, and 4-fluoro nitro benzene, shows appreciable reactivity (Table 3, entries 3–5). Furthermore, the disubstituted rings also show good reactivity under the optimized photochemical reaction conditions (Table 3, entries 7 and 8).

As per the literature, a plausible mechanism is (previously published reports²⁴) shown in Scheme 5. After absorption of visible light (>420 nm), excited electrons transfer from the g-C₃N₄ to the doped Pd (band gap ~2.0–2.5 eV) center enriching the electron density over the Pd centre to initiate the hydrogenation reaction steps.^{24a,b,25} The activated Pd-g-C₃N₄ surface (*via* absorbed visible light) is capable of activating absorbed H₂O molecules (*via* -NH- and -NH₂ active sites of g-C₃N₄) to Mg to form an activated Mg-H₂O complex over Pd-g-C₃N₄ (Scheme 5). Eventually, Mg donates electrons to H₂O to generate H₂ and Mg(OH)₂ simultaneously.^{12c} Furthermore, Mg(OH)₂ activated again with the



Scheme 5 Probable mechanism for Pd-g-C₃N₄ catalyzed photocatalytic hydrogenation reaction.

Table 3 Nitro group reduction *via* the Pd-g-C₃N₄ photocatalyst

Entry	Substrate	Product	Yield (%)
1			95
2			90
3			100
4			99
5			99
6			80
7			90
8			90

Reaction conditions: Substrate (10 mmol), Mg powder (15 mmol, 0.364 g), NiCl₂ (0.1 mmol, 0.129 g), Pd-g-C₃N₄, 30 mg (0.8 wt% Pd, 0.0022 mmol), and water (10 mL) solvent, under visible light (15 W LED lamp, 12 cm height).

help of a catalytic amount of NiCl₂ in the reaction mixture (Scheme 5).^{12c}

To support the fact that water really acts as a hydrogen source, we performed the hydrogenation reaction (see the details in the ESI†) with D₂O solvent in place of H₂O solvent with both the substrate olefin and nitro group hydrogenation under the optimized reaction conditions (see ESI, Fig. S8 and S9†).^{12a} Experiments carried out with D₂O as the solvent resulted in 60% and 55% yield of deuterated ethylbenzene and 4-amino toluene, respectively^{12a} (confirmed *via* GC-MS analysis), clearly suggesting that water is the only source of H₂ generation for the photo-hydrogenation described here (Fig. S9†).

The observed water contact angle for the Pd-g-C₃N₄ catalyst surface is 19.7°. As per the Cassie and Wenzel model, a material with a water contact angle of more than 90° is classified as hydrophobic, whereas that showing a contact angle less than 90° is categorized as hydrophilic.²⁷ This supports the fact that Pd-g-C₃N₄ can absorb water molecules easily due to the presence of -NH- and -NH₂ active sites along with hydrogen bonding and van der Waals forces over the g-C₃N₄ surface (Fig. S10†). The recycling study results of the photocatalyst Pd-g-C₃N₄ for (A) olefin (styrene) (B) and nitro group (4-nitro toluene) hydrogenation are shown in Fig. 2.

For a better understanding of the process, the reaction kinetics was measured as shown in Fig. 2. To evaluate the optimum size for the Mg particle, we screened three different sizes 0.08–0.1 μm, 0.1–0.5 μm and 0.5–1.5 μm (Fig. 2A). The results suggest that the most active size is 0.1–0.5 μm. The available surface area of Mg is a crucial factor for Mg-H₂O complex formation. In another reaction kinetics profile, we examined the reaction progress at three different stirring speeds 600, 800, and 1000 rpm (Fig. 2B). Since the reaction mixture is heterogeneous in nature (Pd-g-C₃N₄ + Mg/H₂O +

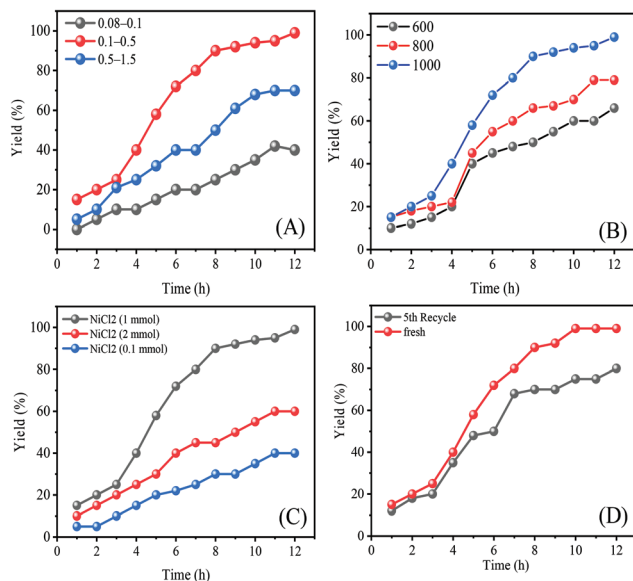


Fig. 2 Pd-g-C₃N₄ photocatalyst reaction kinetics profile for the photo-reaction; (A) Mg particle size (μm) impact, (B) stirring speed effects, (C) co-catalyst NiCl₂ amount impact, and (D) fresh and reused catalyst comparison.

NiCl₂), the reaction stirring speed plays a highly crucial role in determining the reaction rate. We found that fast stirring was essential for the reaction rate (1000 rpm for 12 h, 99% yield) (Fig. 2B). In the next set of experiments, we modified the amount of NiCl₂ added to the reaction, 1 mmol, 2 mmol, and 0.1 mmol were screened (Fig. 2C). Since the amount of NiCl₂ plays a crucial role here in the Mg regeneration from MgO (Scheme 2), the reaction progress exhibits strong dependence on the Ni amount. In the next screening, we used a fresh and reused catalyst, to realize that the photocatalyst is highly active even after the 5th recycle (Fig. 2D).

We recycled and reused the Pd-g-C₃N₄ photocatalyst several times which does not show any major change in its activity (100–80% conversion) in both photo-reactions²⁸ (Fig. 3). After the photochemical reaction was complete the solid photocatalyst Pd-g-C₃N₄ was separated *via* filtration with Whatman filter paper, consequently washed with methanol and acetone alternately five times and further oven dried (100 °C, overnight). From Fig. 3, it is clear that the Pd-g-C₃N₄ photocatalyst could be reused many times without any change in its activity and the product yield remained good for both the hydrogenation reactions Fig. 3A and B (ESI, 1c†) (olefin and nitro group conversion).

We performed Sheldon's hot filtration test to test the heterogeneous nature and stability performance of the synthesized Pd-g-C₃N₄ photocatalyst (see ESI, Fig. S11†). The observed results have shown nearly negligible Pd leaching into the reaction solution during the course of the process. To perform Sheldon's hot filtration test for the optimized photochemical hydrogenation reaction conditions, the photo-catalyst Pd-g-C₃N₄ was filtered out from the reaction mixture after 2 h of the photo-reaction. The reaction filtrate was again trans-

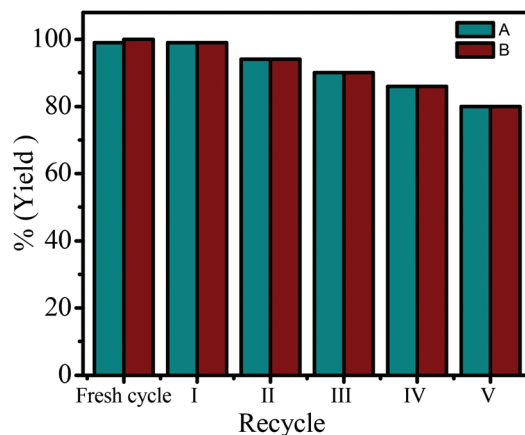


Fig. 3 Recycling study for the Pd-g-C₃N₄ photocatalyst. (A) Styrene hydrogenation, (B) Nitrobenzene hydrogenation (Under optimized reaction conditions).

ferred into the pressure tube for further continuation of the reaction without the photo-catalyst (fresh addition of the Mg reagent and Ni catalyst). GC analysis of the filtrate confirmed that the conversion was up to 42% of the corresponding products, respectively (styrene to methylbenzene). After a 2 h time span, the conversion is 42% and after removal of the catalyst it reaches up to 45% conversion (which might be due to fresh addition of the Mg reagent and Ni co-catalyst). But proceeding further with the unavailability of the Pd-g-C₃N₄ catalyst makes the progress of the reaction very slow. As confirmed by GC analysis, there was no improvement in the yield (<45% yield) of the hydrogen transferred product (styrene to ethylbenzene), even with prolongation of the hot filtrate reaction by an additional 12 h under visible light (see ESI, Fig. S11†).

For the molecular level analysis of the recycled Pd-g-C₃N₄ photo-catalyst, XRD characterization was carried out. The performed characterization suggests that the five times recycled Pd-g-C₃N₄ photocatalyst remains unchanged at the molecular level with the persistence of diffraction peaks indexed at the (100) plane at 13.4° and at the (002) plane at 27.2° even after multiple reuses (see ESI, Fig. S12†). BET characterization after 5 times recycled Pd-g-C₃N₄ shows a surface area (BET) of 6.975 m² g⁻¹, a total pore volume (V_p) of 0.012 cc g⁻¹ and a mean pore size (radius) D_v(r) of 15.368 Å. The observed decrease in surface area, pore volume and pore size might be due to the continuous use of the reagent and co-catalyst (see ESI, Fig. S13A and B†). XPS analysis exhibits the persistence of the Pd(0) oxidation state with Pd 3d_{5/2} and Pd 3d_{3/2} at 335.0 eV and at 340.2 eV, respectively (see ESI Fig. S14A†). Pyridine-N species [sp²-hybridized nitrogen (C=N-C) at 398.9, amino functional groups (C-N-H) at 400.1 and terminal amino groups (-NH) group at 401.46 eV] well observed in the 5 times recycled Pd-g-C₃N₄ photocatalyst confirm well the N characteristic binding energy (see ESI, S14B†). In addition, SEM analysis of the 5 times recycled Pd-g-C₃N₄ photocatalyst shows a well maintained unchanged smaller unit of agglomeration with denser morphology (see ESI, S15†). FT-IR analysis of the

reused Pd-g-C₃N₄ catalyst (five recycles) was carried out to find out the change of Pd-g-C₃N₄ at the molecular level. Fig. S16† shows that the triazine repeating units at 810 cm⁻¹ vibration modes are well preserved even after multiple reuses with other characteristic IR absorption bands. (see ESI, S16†).

Conclusions

In conclusion, we successfully devised a selective, sustainable, non-hazardous and mild photochemical protocol for the efficient reduction of alkenes to alkanes and nitro compounds *via* Mg-activated water as a H₂ source in the presence of a Pd-g-C₃N₄ photocatalyst at room temperature. Pd-g-C₃N₄ under photochemical conditions successfully excluded the usage of high pressure hydrogen which is highly explosive in nature, making the newly developed protocol a clearly novel green process for hydrogenation with Mg-H₂O as the H₂ source. The use of water, which is the only environmentally benign and inexpensive solvent, makes the developed process a replacement for several existing procedures. In a greener way, the present method could be the most prominent, economical, nontoxic byproduct and efficient, hazardous waste generation free approach towards the reduction of alkenes and the nitro group selectively.

Experimental

Graphitic carbon nitride (g-C₃N₄) and Pd-g-C₃N₄ photocatalyst synthesis

g-C₃N₄ was synthesized by a known method as reported by J. by Wei Chen¹⁴ using urea (10 g) at 550 °C for 3 h (10 °C min⁻¹). Yield (0.80 g). Pd-g-C₃N₄ was fabricated using PdCl₂ in H₂O and preheated g-C₃N₄ with a catalytic amount of potassium formate at 800 rpm for 24 h (ESI: SE a-d†) (Scheme 1).

Hydrogenation using the photocatalyst Pd-g-C₃N₄

A mixture of the substrate (1.0 mmol), Mg powder (1.5 mmol, 0.364 g), NiCl₂ (0.1 mml, 0.129 g), Pd-g-C₃N₄ 30 mg (0.4 wt% Pd, 0.0012 mmol), and water (10 mL) was placed in a pressure glass tube equipped with a magnetic stirrer and was degassed under a flow of nitrogen for five minutes. After completion of the reaction, the samples were diluted with dichloromethane (DCM) and filtered using Whatman paper before injection into a GC (Fig. S2†).

Conflicts of interest

There are no conflicts to declare.

Acknowledgements

The authors acknowledge Hani Gnyayem and Ofer Lahad for their help in present research. Authors thank Dr R. K. Bera for measuring Pd-g-C₃N₄ & water contact angle.

Notes and references

- (a) J. Paradies, *Angew. Chem., Int. Ed.*, 2014, **53**, 3552–3557; (b) C. Gerardo, A. Vanina and L. Carlos, *J. Chem. Technol. Biotechnol.*, 2017, **92**, 27–42.
- J. Tan, J. Cui, X. Cui, T. Deng, X. Li, Y. Zhu and Y. Li, *ACS Catal.*, 2015, **5**, 7379–7384.
- (a) S. Niaz, T. Manzoor and A. H. Pandith, *Renewable Sustainable Energy Rev.*, 2015, **50**, 457–469; (b) N. Armaroli and V. Balzani, *ChemSusChem*, 2011, **4**, 21–36.
- (a) H. Gnyayem and Y. Sasson, *ACS Catal.*, 2013, **3**, 186–191; (b) H. Gnyayem, A. Dandapat and Y. Sasson, *Chem. – Eur. J.*, 2016, **22**, 370–375; (c) H. Gnyayem and Y. Sasson, *J. Phys. Chem. C*, 2015, **119**, 19201–19209.
- (a) K. Maeda, *J. Photochem. Photobiol., C*, 2011, **12**, 237–268; (b) R. Abe, *J. Photochem. Photobiol., C*, 2010, **11**, 179–209; (c) Z. Li, C. Kong and G. Lu, *J. Phys. Chem. C*, 2016, **120**, 56–63; (d) K. Maeda, X. Wang, Y. Nishihara, D. Lu, M. Antonietti and K. Domen, *J. Phys. Chem. C*, 2009, **113**, 4940–4947; (e) A. A. Ismail and D. W. Bahnemann, *Sol. Energy Mater. Sol. Cells*, 2014, **128**, 85–101; (f) M. Ni, M. K. H. Leung, D. Y. C. Leung and K. Sumathy, *Renewable Sustainable Energy Rev.*, 2007, **11**, 401–425; (g) C. A. Grimes, O. K. Varghese and S. Ranjan, in *Light, Water, Hydrogen: The Solar Generation of Hydrogen by Water Photoelectrolysis*, ed. C. A. Grimes, O. K. Varghese and S. Ranjan, Springer US, Boston, MA, 2008, pp. 35–113.
- B. Zhou, J. Song, H. Zhou, T. Wu and B. Han, *Chem. Sci.*, 2016, **7**, 463–468.
- C. Schafer, C. J. Ellstrom, H. Cho and B. Török, *Green Chem.*, 2017, **19**, 1230–1234.
- (a) L. Ouyang, M. Ma, M. Huang, R. Duan, H. Wang, L. Sun and M. Zhu, *Energies*, 2015, **8**, 4237; (b) Y. Liu, X. Wang, H. Liu, Z. Dong, G. Cao and M. Yan, *J. Power Sources*, 2014, **251**, 459–465; (c) R. R. Bhosale, R. V. Shende and J. A. Puszynski, *Int. Rev. Chem. Eng.*, 2010, **2**, 852–862; (d) D. P. Ojha, K. Gadde and K. R. Prabhu, *Org. Lett.*, 2016, **18**, 5062–5065.
- J. Jitputti, S. Pavasupree, Y. Suzuki and S. Yoshikawa, *J. Solid State Chem.*, 2007, **180**, 1743–1749.
- (a) P. Sharma and Y. Sasson, *Green Chem.*, 2017, **19**, 844–852; (b) Y. Wang, X. Wang and M. Antonietti, *Angew. Chem., Int. Ed.*, 2012, **51**, 68–89; (c) X. Wang, K. Maeda, A. Thomas, K. Takanabe, G. Xin, J. M. Carlsson, K. Domen and M. Antonietti, *Nat. Mater.*, 2009, **8**, 76–80.
- (a) A. Thomas, A. Fischer, F. Goettmann, M. Antonietti, J.-O. Muller, R. Schlögl and J. M. Carlsson, *J. Mater. Chem.*, 2008, **18**, 4893–4908; (b) H. Dai, X. Gao, E. Liu, Y. Yang, W. Hou, L. Kang, J. Fan and X. Hu, *Diamond Relat. Mater.*, 2013, **38**, 109–117.
- (a) R. D. Patil and Y. Sasson, *Asian J. Org. Chem.*, 2015, **4**, 1258–1261; (b) R. D. Patil and Y. Sasson, *Appl. Catal., A*, 2015, **499**, 227–231; (c) O. Muhammad, S. U. Sonavane, Y. Sasson and M. Chidambaram, *Catal. Lett.*, 2008, **125**, 46–

- 51; (d) M. Baidossi, A. V. Joshi, S. Mukhopadhyay and Y. Sasson, *Synth. Commun.*, 2004, **34**, 643–650.
- 13 I. A. Taub, W. Roberts, S. LaGambina and K. Kustin, *J. Phys. Chem. A*, 2002, **106**, 8070–8078.
- 14 J. Liu, T. Zhang, Z. Wang, G. Dawson and W. Chen, *J. Mater. Chem.*, 2011, **21**, 14398–14401.
- 15 L. Zhang, A. Wang, J. T. Miller, X. Liu, X. Yang, W. Wang, L. Li, Y. Huang, C.-Y. Mou and T. Zhang, *ACS Catal.*, 2014, **4**, 1546–1553.
- 16 (a) S. Cao and J. Yu, *J. Phys. Chem. Lett.*, 2014, **5**, 2101–2107; (b) H. Shi, G. Chen, C. Zhang and Z. Zou, *ACS Catal.*, 2014, **4**, 3637–3643; (c) Y. Shiraishi, S. Kanazawa, Y. Sugano, D. Tsukamoto, H. Sakamoto, S. Ichikawa and T. Hirai, *ACS Catal.*, 2014, **4**, 774–780.
- 17 (a) K. Wu, Y. Cui, X. Wei, X. Song and J. Huang, *J. Saudi Chem. Soc.*, 2015, **19**, 465–470; (b) X. Bai, L. Wang, R. Zong and Y. Zhu, *J. Phys. Chem. C*, 2013, **117**, 9952–9961; (c) W.-J. Ong, L.-L. Tan, S.-P. Chai and S.-T. Yong, *Dalton Trans.*, 2015, **44**, 1249–1257.
- 18 F. Dong, Z. Wang, Y. Li, W.-K. Ho and S. C. Lee, *Environ. Sci. Technol.*, 2014, **48**, 10345–10353.
- 19 (a) X. Shao, J. Xu, Y. Huang, X. Su, H. Duan, X. Wang and T. Zhang, *AIChE J.*, 2016, **62**, 2410–2418; (b) A. Kumar, P. Kumar, C. Joshi, S. Ponnada, A. K. Pathak, A. Ali, B. Sreedhar and S. L. Jain, *Green Chem.*, 2016, **18**, 2514–2521.
- 20 J. Ren, X. Liu, L. Zhang, Q. Liu, R. Gao and W.-L. Dai, *RSC Adv.*, 2017, **7**, 5340–5348.
- 21 Y. Wang, J. Yao, H. Li, D. Su and M. Antonietti, *J. Am. Chem. Soc.*, 2011, **133**, 2362–2365.
- 22 S. Mukhopadhyay, G. Rothenberg, H. Wiener and Y. Sasson, *New J. Chem.*, 2000, **24**, 305–308.
- 23 J. Zheng, D. Yang, W. Li, H. Fu and X. Li, *Chem. Commun.*, 2013, **49**, 9437–9439.
- 24 (a) S. Ye, R. Wang, M.-Z. Wu and Y.-P. Yuan, *Appl. Surf. Sci.*, 2015, **358**, 15–27; (b) S. Yin, J. Han, T. Zhou and R. Xu, *Catal. Sci. Technol.*, 2015, **5**, 5048–5061; (c) Y.-P. Zhu, T.-Z. Ren and Z.-Y. Yuan, *ACS Appl. Mater. Interfaces*, 2015, **7**, 16850–16856.
- 25 (a) L. K. Putri, W.-J. Ong, W. S. Chang and S.-P. Chai, *Appl. Surf. Sci.*, 2015, **358**(Part A), 2–14; (b) X. Chen, J. Zhang, X. Fu, M. Antonietti and X. Wang, *J. Am. Chem. Soc.*, 2009, **131**, 11658–11659.
- 26 (a) R. Shamai, D. Andelman, B. Berge and R. Hayes, *Soft Matter*, 2008, **4**, 38–45; (b) S. Arscott, *RSC Adv.*, 2014, **4**, 29223–29238.
- 27 Y. Ma, X. Cao, X. Feng, Y. Ma and H. Zou, *Polymer*, 2007, **48**, 7455–7460.
- 28 (a) P. Sharma and A. P. Singh, *RSC Adv.*, 2014, **4**, 58467–58475; (b) C. Hammond, *Green Chem.*, 2017, **19**, 2846–2854; (c) P. Sharma and A. P. Singh, *Catal. Sci. Technol.*, 2014, **4**, 2978–2989.